Landau Level Splittings, Phase Transitions, and Nonuniform Charge Distribution in Trilayer Graphene

Leonardo C. Campos,[1] Thiti Taychatanapat,[2] Maksym Serbyn,[3] Kawin Surakitbovorn,[4] Kenji Watanabe,[5] Takashi Taniguchi,[5] Dmitry A. Abanin,[6] and Pablo Jarillo-Herrero[4,*]

[1]*Departamento de Fisica, Universidade Federal de Minas Gerais, Belo Horizonte, Minas Gerais 31270-901, Brazil*
[2]*Department of Physics, Faculty of Science, Chulalongkorn University, Patumwan, Bangkok 10330, Thailand*
[3]*Department of Physics, University of California, Berkeley, California 94720, USA*
[4]*Department of Physics, Massachusetts Institute of Technology, Cambridge, Massachusetts 02139, USA*
[5]*Advanced Materials Laboratory, National Institute for Materials Science, 1-1 Namiki, Tsukuba 305-0044, Japan*
[6]*Department of Theoretical Physics, University of Geneva, 1211 Genève 4, Switzerland*

We report on magnetotransport studies of dual-gated, Bernal-stacked trilayer graphene (TLG) encapsulated in boron nitride crystals. We observe a quantum Hall effect staircase which indicates a complete lifting of the 12-fold degeneracy of the zeroth Landau level. As a function of perpendicular electric field, our data exhibit a sequence of phase transitions between all integer quantum Hall states in the filling factor interval $-8 < \nu < 0$. We develop a theoretical model and argue that, in contrast to monolayer and bilayer graphene, the observed Landau level splittings and quantum Hall phase transitions can be understood within a single-particle picture, but imply the presence of a charge density imbalance between the inner and outer layers of TLG, even at charge neutrality and zero transverse electric field. Our results indicate the importance of a previously unaccounted band structure parameter which, together with a more accurate estimate of the other tight-binding parameters, results in a significantly improved determination of the electronic and Landau level structure of TLG.

The electronic properties of *ABA*-stacked trilayer graphene (TLG) are being intensively investigated [1–6] due to its distinct band structure which consists of two overlapping monolayer-graphene-like (MLG-like) and bilayer-graphene-like (BLG-like) bands [1,7–14]. However, in contrast to MLG and BLG, which are gapless, both subbands in *ABA*-stacked TLG are gapped, with small masses of the order of a few meV.

One of the most interesting characteristics of *ABA*-stacked TLG compared to other graphene systems is the way in which its band structure is modified by a perpendicular electric field [2,12,14–18]. Theory predicts that a weak electric field hybridizes the MLG-like and BLG-like bands, rather than inducing a band gap, as in BLG or *ABC*-stacked TLG [3,16,19–21]. The hybridized bands are characterized by a strong trigonal warping. For very strong electric fields, a new set of Dirac points was theoretically predicted, with masses and velocities that are controlled by the electric field [18,22]. Thus *biased* TLG can potentially provide an opportunity to study chiral carriers with tunable anisotropic dispersion, different symmetry, and higher valley degeneracy (6 as opposed to two in MLG and BLG), not accessible in MLG and BLG.

Here we report on transport studies of high-mobility TLG samples in the quantum Hall effect regime. We fabricated dual-gated TLG samples encapsulated in hexagonal boron nitride [23,24] crystals (*h*BN) [Figs. 1(a)–1(b)], which

allowed us to independently control the carrier density n and perpendicular electric displacement field D. We use magnetotransport measurements to study how Landau levels (LLs) evolve under D. By inspecting the pattern of LL crossings resulting from the hybridization of the BLG-like and MLG-like bands as a function of n, D, and magnetic field B, we are able to refine the values of the TLG band structure parameters.

Additionally, we observe a quantum Hall staircase with plateaus spaced by e^2/h, indicating a complete lifting of the low-lying LL degeneracies [25–28]. We find a number of D-driven phase transitions between different integer quantum Hall (QH) states within the zeroth LL. The phase transitions occur at every integer filing factor in the interval $-8 \leq \nu \leq 0$. While in MLG and BLG the zeroth LL splittings usually arise from Coulomb interaction effects, we argue that the splittings and phase transitions that we observe are consistent with a single-particle picture. We develop a theoretical model and show that the observed phase transitions can be attributed to multiple LL crossings induced by the transformation of the TLG band structure under D. However, the sequence of phase transitions implies a finite value for a previously neglected parameter in the band structure, which corresponds to the difference of electrostatic potential of the middle layer from the average potential on outer layers of TLG. Such a term, allowed by symmetry, points to a nonuniform internal
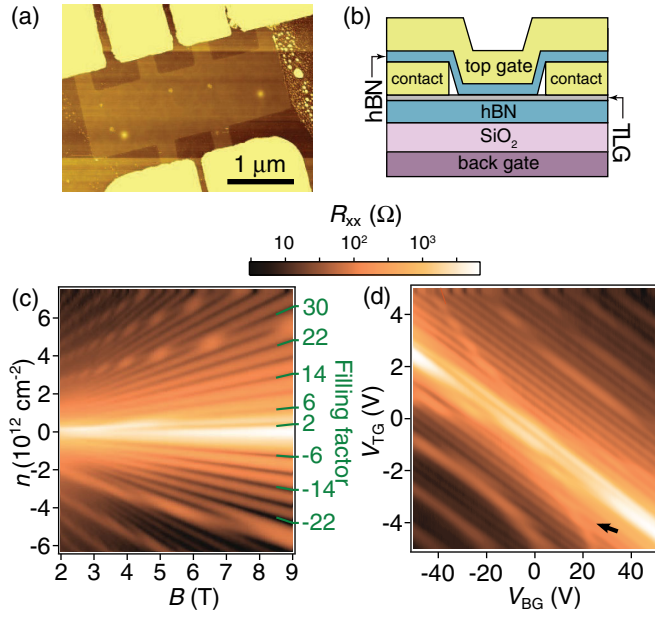
FIG. 1. (a) AFM image of device 1 four probe Hall bar geometry before top gate preparation. The length and width of device 1 are 3 μm and 1 μm, respectively. (b) Schematic sketch of the sample showing the configuration of top gate and back gate electrodes. (c) R_{xx} as a function of n and B at $D = 0$. (d) R_{xx} as a function of top gate and back gate voltages at $B = 4$ T. The black arrow points to the quickly dispersing LL crossings at $D \neq 0$ on the electron side. These LL crossings also occur on the hole side. Data in (c) and (d) are measured at 4 K.

electric field in TLG, which is caused by *nonzero charge density* on the middle layer. In particular, even at the charge neutrality and zero D there are nonzero charges on outer and inner layers [12], see Fig. 2.

Our devices are fabricated using hBN crystals as a local substrate to improve device quality [23]. Then another hBN flake is transferred on top of TLG to cover the sample [Figs. 1(a)–1(b)] [17]. This allows us to fabricate a top gate, enabling the independent control of both n and D. These two quantities can be related to the voltages on the top and
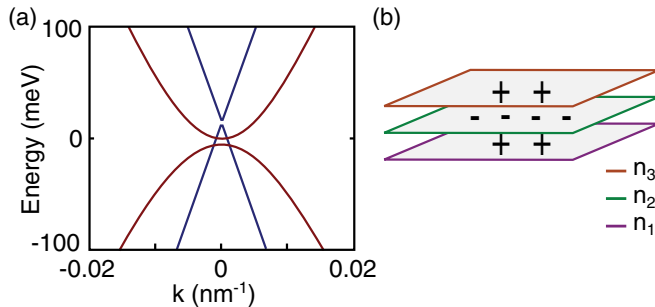

FIG. 2. (a) Band structure of TLG for $\gamma_0 = 3.1$ eV, $\gamma_1 = 0.39$ meV, $\gamma_2 = -18$ meV, $\gamma_3 = 315$ meV, $\gamma_4 = 100$ meV, $\gamma_5 = 10$ meV, $\delta = 15$ meV, $\Delta_1 = 0$, and $\Delta_2 = 1.8$ meV. (b) Schematic cartoon showing charge distribution at $\Delta_1 = 0$ and $n = 0$.

bottom gates, V_{TG}, V_{BG}, via $n = (C_{TG}V_{TG} + C_{BG}V_{BG})/e$ and $D = (C_{TG}V_{TG} - C_{BG}V_{BG})/2$, where C_{TG}, C_{BG} are the top gate and back gate capacitances per unit of area. We have measured two TLG devices, one in a Hall bar geometry (device 1) and the other in a two-terminal geometry (device 2).

To establish that our graphene devices indeed consist of *ABA*-stacked TLG, we first studied magnetotransport at $D = 0$, where the MLG-like and BLG-like bands are not hybridized. The longitudinal resistance R_{xx}, shown in Fig. 1(c), exhibits minima at many integer filling factors, indicating the high quality of the device. More importantly, characteristic crossings between MLG-like and BLG-like LLs are evident, which originate from the different scaling of LL energies with B: ignoring small mass terms, LL energies scale as $\sqrt{B}$ and B for MLG-like and BLG-like bands, respectively [2,9,10,29–32].

The pattern of LL crossings in Fig. 1(c) is qualitatively similar to that observed in Ref. [2], but there are two new important features. First, at high electron density, the locations of LL crossings at fixed B are different, with the crossing points shifted up by one (fourfold degenerate) LL compared to Ref. [2]. For example, at $B = 9$ T, we observe the LL crossing point at filling factor $\nu = 26$ instead of $\nu = 22$ as it was reported in Ref. [2]. We note that, at high hole density $n < -2 \times 10^{12}$ cm^{-2}, values of n and B at which LL crossings occur are very similar to those in Ref. [2]. The difference in the LL crossing locations on the electron side is due to the different electrostatic conditions of experiment [2], which was performed at small $D(n) \neq 0$. The second and more important difference occurs at low density. In particular, it is evident that the zeroth LL (which, in the simplified tight-binding model, is 12-fold degenerate) is partially split, and this splitting breaks electron-hole symmetry. This can be seen in Fig. 1(c) for 4T $< B <$ 9 T: there is a clear minimum of R_{xx} for filling factor $\nu = +2$ but not for $\nu = -2$. These new features at low and high charge density indicate that the TLG tight-binding parameters have to be reevaluated. In particular, we will see below that a nonzero parameter Δ_2, describing the charge redistribution between the central and outer layers, is necessary to explain the electron-hole asymmetry observed at filling factor $\nu = \pm 2$.

Next, we study magnetotransport at $D \neq 0$. The behavior of R_{xx} in device 1 as a function of V_{TG} and V_{BG}, illustrated in Fig. 1(d), reveals a series of LL crossings which occur as a function of bias at fixed B. Theoretically, such crossings are expected as a result of the LL structure modification induced by the hybridization of MLG-like and BLG-like bands. Notice that LL crossings are visible on both electron and hole sides.

Since disorder-induced LL broadening (most likely due to charge inhomogeneity) prevents us from resolving the fine structure of LL crossings as a function of D, we turn to device 2, which had a much smaller charge inhomogeneity.
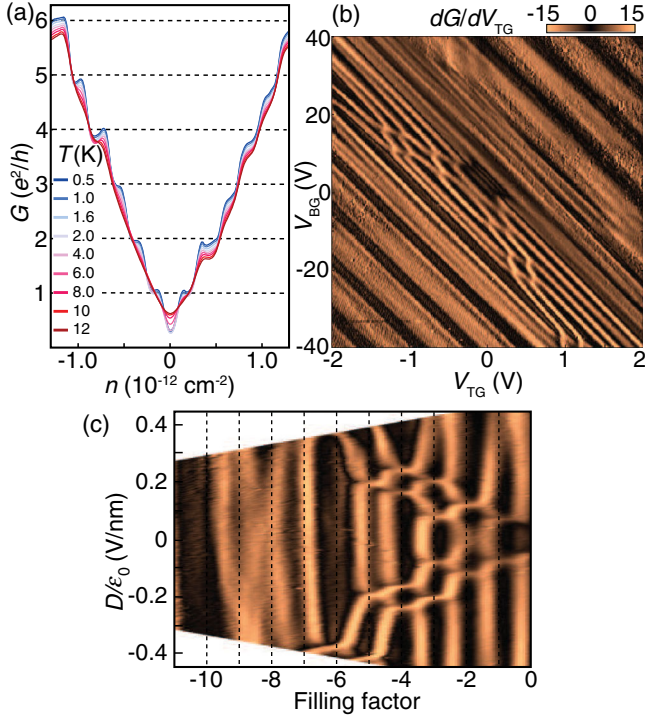
FIG. 3. (a) Conductance plateaus at $B = 9$ T as function of charge density at various temperature. The length and width of device 2 are 3 μm and 4 μm, respectively. (b) Numerical derivative of the conductance at $B = 9$ T. (c) Zoom in data shown in (b), showing the crossing of LLs, plotted vs filling factor, ν and D/ε_0, where ε_0 is the vacuum permittivity. Data in (b) and (c) are measured at 300 mK.

The two-terminal conductance of device 2 at $B = 9$ T and $D = 0$ shows a quantum Hall effect staircase with plateau spacing e^2/h, indicating a complete splitting of the zeroth and first LL [Fig. 3(a)]. It is important to note that the plateaus are better developed on the hole side, where a complete splitting for $-10 \leq \nu < 0$ is visible. On the electron side, only a partial splitting is found, and the plateaus are not as pronounced, which we believe to be the result of electron-hole asymmetric disorder effects.

Next, we explored the behavior of split LLs at finite D. Figure 3(b) shows differential conductance dG/dV_{TG} as a function of top gate and back gate voltages. It is convenient to replot differential conductance as a function of D and filling factor ν [Fig. 3(c)]. This plot reveals symmetrical crossings at all filling factors in the interval $-8 < \nu \leq -1$ for positive and negative D. Clearly, as $|D|$ is increased, a pair of LLs quickly shifts away from zero energy, crossing other LLs. This results in a series of QH phase transitions. Note that a similar experiment has been performed by Lee *et al.* [6] but the quantum Hall staircase details were obscured by charge inhomogeneity. This behavior is also observed in device 1—see Fig. 1(d), where the quickly shifting pair of LLs (which are merged together due to disorder broadening) is pointed by a black arrow. Besides, in device 2, there might be a crossing at $\nu = 0$ at very small D, but we were not able

to fully resolve it. We leave the nature of $\nu = 0$ and its transformations with D for future studies.

To understand the LL crossings above, we calculate the *single-particle* LL spectrum as a function of D and B numerically, and show that theory captures all the key observed features—locations of LL crossings, splitting of the zeroth LL, as well as phase transitions between different QH states. We argue that in order to faithfully describe the data, it is necessary to include a term Δ_2 in the tight-binding model of TLG, and moreover, we refine the values of the other tight-binding parameters.

To describe the band structure of trilayer graphene, we use the Slonczewski-Weiss-McClure parametrization of the tight-binding model [12,18], which includes seven parameters ($\gamma_0, \ldots, \gamma_5, \delta$). Also, to describe the effect of D, we introduce the on-site potentials on the three TLG layers, U_1, U_2, U_3. Since only potential differences are meaningful, it is convenient to define parameters

$$\Delta_1 = (-e)(U_1 - U_3)/2, \quad \Delta_2 = (-e)(U_1 - 2U_2 + U_3)/6.$$

Parameter Δ_1 describes the potential difference between the two outer layers, and it is zero at $D = 0$. However, parameter Δ_2, describing the potential difference between the central layer and the average of the outer layers, is allowed by symmetry even at $D = 0$. The presence of $\Delta_2 \neq 0$ without displacement field indicates nonzero charge on the middle layer, which is obviously disfavored by electrostatic energy, and arises from the interplay between band structure and electrostatics.

We can confirm the existence of Δ_2 at low density by considering the Landau gaps at $\nu = +2$ and $\nu = -2$. These two gaps are given by $\Delta\varepsilon_2 = +3\Delta_2 - \gamma_2/2$ and $\Delta\varepsilon_{-2} = -3\Delta_2 - \gamma_2/2$, where γ_2 is the tight-binding parameter associated with the hopping integral between A sites in the outer layers ($A_1 \leftrightarrow A_3 : \gamma_2$) [12,18]. In device 1, we observe a splitting at $\nu = 2$ but not at $\nu = -2$ [Fig. 1(c)]. This implies that Δ_2 is greater than zero or, equivalently, the gap at $\nu = 2$ is larger than that at $\nu = -2$. We note that the gap at $\nu = -2$ is nonzero. However, we do not observe the splitting at $\nu = -2$ in device 1 due to disorder broadening. In device 2, which has a better quality than device 1, we are able to resolve the gap at $\nu = -2$.

We also find the values of the tight-binding parameters which best reproduce the locations of LL crossings at $D = 0$ [Fig. 1(c)]. Parameter Δ_2 is expected to depend on the charge density, since additional charge can also distribute asymmetrically among central and outer layers. Therefore, in our analysis Δ_2 needs to be reevaluated for each density of charge, to describe electron-hole asymmetries at low charge density (see more details in Supplemental Material [33]). The other parameters are taken from fitting of the crossing patterns at high charge density, see Table I.

Next, we explain the LL splittings and fast diving of two LLs away from zero energy with increasing D observed in Fig. 3(c). The Landau levels are shown in Fig. 4(a), where

TABLE I. Tight-binding parameters obtained by fitting the pattern of Landau level crossings shown in Fig. 1(c)

γ_0 (eV)	γ_1 (eV)	γ_2 (meV)	γ_3 (meV)	γ_4 (meV)	γ_5 (meV)	δ (meV)
3.1	0.39	−20 to −16	315	40 to 140	5 to 15	12 to 18

MLG-like bands are in red lines and BLG-like bands are in blue lines. First let us discuss the splitting of the zeroth LL at $D = 0$. Ignoring the spin degree of freedom, the zeroth LL consists of six sublevels. Two sublevels originate from the MLG-like band, labeled $0^m_\pm$, and have the highest (and positive) energies [see Fig. 4(b)]:

$$E_{0^m_+} = \delta - \frac{1}{2}\gamma_5 + \Delta_2, \qquad E_{0^m_-} = -\frac{1}{2}\gamma_2 + \Delta_2,$$

where $\pm$ labels the two valleys. The four remaining sublevels originate from the BLG-like band [four blue lines closest to zero energy in Fig. 4(b)], with energies

$$E_{0^b_+} \approx E_{1^b_+} \approx -2\Delta_2 + \delta E_{01}^+, \tag{1}$$

$$E_{0^b_-} \approx E_{1^b_-} \approx \frac{1}{2}\gamma_2 + \Delta_2 + \delta E_{01}^-, \tag{2}$$

where $\delta E_{01}^\pm$ denotes small single-particle splittings between the 0,1 sublevels within the corresponding valley [18]. The spin degeneracy is lifted by the Zeeman interaction, $E_Z = g\mu_B B \approx 10$ K at $B = 10$ T. Thus, the zeroth LL is fully split. The gaps estimated by numerical solutions are of the order of a few meV, except for the gap at $\nu = 2$ (all BLG-like sublevels filled) $\Delta E \sim 15$ meV. The size of the single-particle gaps is consistent with the observed
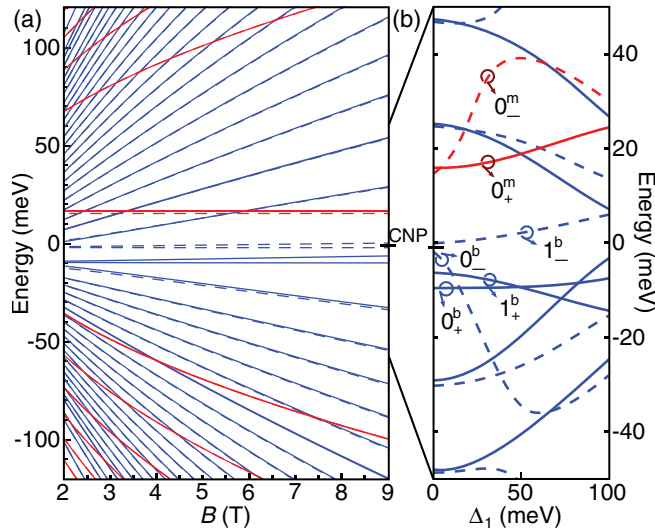

FIG. 4. (a) Numerical simulation of the LL spectrum. Red lines are solutions for MLG-like LLs, solid lines address valley K and dashed lines address valley K_. Blue lines are solutions for BLG-like LLs, solid lines address valley K and dashed lines address valley K_. (b) LL crossing as function average interlayer potential difference Δ_1.

temperature scale at which the QH states in the interval $0 < |\nu| < 6$ disappear ($T \sim 10$ K).

Below we focus on the region $-6 < \nu < 0$, where D-induced phase transitions occur. Filling factor $\nu = 0$ corresponds to filling 6 sublevels in the BLG-like sector. When the displacement field is applied, the BLG-like and MLG-like bands can no longer be treated as independent, they hybridize, and the effect of trigonal warping increases. These band structure changes lead to a rearrangement of the Landau sublevels. In the interval of D values corresponding to $0 < |\Delta_1| < 30$ meV, achieved in our experiment, the main effect is that the 0^b_- LL [dashed blue line just below the charge neutrality point (CNP) in Fig. 4(b)] rapidly sinks down in energy, while LL 1^b_- slowly shifts up in energy. Landau levels 0^b_+, 1^b_+ disperse rather weakly.

Thus, the phase transitions observed for $-6 < \nu < 0$ can be understood as the result of the spin-split 0^b_- LL crossing the spin-split 0^b_+, 1^b_+ LLs. This implies that at $D = 0$, $E_{0^b_-} > \max(E_{0^b_+}, E_{1^b_+})$, which puts a limitation on the value of Δ_2. From Eqs. (1) and (2), we obtain an estimate

$$\Delta_2 > -\gamma_2/6 \approx 2.7 \text{ meV}. \tag{3}$$

The phase transition observed at $\nu = -1$ is attributed to the crossing between $0^b_-\downarrow$ and $1^b_-\uparrow$ levels (the Zeeman interaction is very likely strong enough to bring the $0^b_-\downarrow$ level above $1^b_-\uparrow$ one at $D = 0$). Upon increasing D, these levels cross. The evolution of LLs and their crossings are shown in Fig. 4(b) for $\Delta_2 = 5.7$ meV.

Our results indicate that parameter Δ_2 is nonzero, implying a nonuniform electric field distribution and the presence of charge on the middle layer of TLG. It is interesting to note that, despite the large impact of Δ_2 on the LL spectrum, its effect on the band structure itself at $B = 0$ is very small. Indeed, the highly degenerate LL with wave functions often localized on particular layers [18] are more sensitive to Δ_2 and can lead to its enhancement within a self-consistent picture. On the other hand, in the continuous band structure, the effect of Δ_2 is barely noticeable. To illustrate this, in Fig. 2(a) we plot the energy dispersion at $B = 0$ and $D = 0$ for $\Delta_2 = 1.8$ meV (value of Δ_2 at $n = 0$ and $B = 9$ T). Figure 2(b) schematically illustrates the nonuniform charge distribution. Essentially, the band structure looks qualitatively the same as that previously reported [2,5,12,17] at $\Delta_2 = 0$ there is an energy band overlap between MLG-like and BLG-like, and the band gap between bilayer subbands is of the order of ~6 meV at $n = 0$. Thus, we need magnetotransport measurements at high field to obtain the value of Δ_2.

In summary, we have measured and calculated the fine structure of Landau levels in *ABA*-stacked, dual-gated trilayer graphene devices. We found full splitting of the zeroth LL, as well as a series of quantum Hall phase transitions induced by electric displacement field. We showed that this behavior is well described by a

single-particle model, once a previously neglected parameter is included in the tight-binding model of TLG. The existence of this parameter implies a nontrivial electric field distribution between the middle and outer layers in TLG caused by the interplay between electrostatic energy and band structure.

Finally, although our findings are consistent with a single-particle model, there is little doubt that TLG should host interesting fractional quantum Hall states, which should become observable in devices with even lower disorder than those presented here. Our studies show that TLG is a material in which LL energies and wave functions are widely tunable by D. In the future it would be interesting to study whether this tunability could be used to control effective interactions and tuning fractional quantum Hall states [36].

L. C. C and T. Taychatanapat contributed equally to this work.

---

*pjarillo@mit.edu

[1] M. F. Craciun, S. Russo, M. Yamamoto, J. B. Oostinga, A. F. Morpurgo, and S. Tarucha, Nat. Nanotechnol. **4**, 383 (2009).

[2] T. Taychatanapat, K. Watanabe, T. Taniguchi, and P. Jarillo-Herrero, Nat. Phys. **7**, 621 (2011).

[3] W. Bao, L. Jing, J. Velasco, Jr., Y. Lee, G. Liu, D. Tran, B. Standley, M. Aykol, S. B. Cronin, D. Smirnov, M. Koshino, E. McCann, M. Bockrath, and C. N. Lau, Nat. Phys. **7**, 948 (2011).

[4] E. A. Henriksen, D. Nandi, and J. P. Eisenstein, Phys. Rev. X **2**, 011004 (2012).

[5] K. Zou, F. Zhang, C. Clapp, A. H. MacDonald, and J. Zhu, Nano Lett. **13**, 369 (2013).

[6] Y. Lee, J. Velasco, D. Tran, F. Zhang, W. Bao, L. Jing, K. Myhro, D. Smirnov, and C. N. Lau, Nano Lett. **13**, 1627 (2013).

[7] S. Latil and L. Henrard, Phys. Rev. Lett. **97**, 036803 (2006).

[8] B. Partoens and F. M. Peeters, Phys. Rev. B **74**, 075404 (2006).

[9] F. Guinea, A. H. Castro Neto, and N. M. R. Peres, Phys. Rev. B **73**, 245426 (2006).

[10] E. McCann and V. I. Fal'ko, Phys. Rev. Lett. **96**, 086805 (2006).

[11] M. Aoki and H. Amawashi, Solid State Commun. **142**, 123 (2007).

[12] M. Koshino and E. McCann, Phys. Rev. B **79**, 125443 (2009).

[13] C. H. Lui, L. Liu, K. F. Mak, G. W. Flynn, and T. F. Heinz, Nature (London) **462**, 339 (2009).

[14] M. Koshino, Phys. Rev. B **81**, 125304 (2010).

[15] M. Koshino and E. McCann, Phys. Rev. B **80**, 165409 (2009).

[16] S. H. Jhang, M. F. Craciun, S. Schmidmeier, S. Tokumitsu, S. Russo, M. Yamamoto, Y. Skourski, J. Wosnitza, S. Tarucha, J. Eroms, and C. Strunk, Phys. Rev. B **84**, 161408 (2011).

[17] L. C. Campos, A. F. Young, K. Surakitbovorn, K. Watanabe, T. Taniguchi, and P. Jarillo-Herrero, Nat. Commun. **3**, 1239 (2012).

[18] M. Serbyn and D. A. Abanin, Phys. Rev. B **87**, 115422 (2013).

[19] C. H. Lui, Z. Li, K. F. Mak, E. Cappelluti, and T. F. Heinz, Nat. Phys. **7**, 944 (2011).

[20] T. Khodkov, F. Withers, D. C. Hudson, M. F. Craciun, and S. Russo, Appl. Phys. Lett. **100**, 013114 (2012).

[21] T. Khodkov, I. Khrapach, M. F. Craciun, and S. Russo, Nano Lett. **15**, 4429 (2015).

[22] T. Morimoto and M. Koshino, Phys. Rev. B **87**, 085424 (2013).

[23] C. R. Dean, A. F. Young, I. Meric, C. Lee, L. Wang, S. Sorgenfrei, K. Watanabe, T. Taniguchi, P. Kim, K. L. Shepard, and J. Hone, Nat. Nanotechnol. **5**, 722 (2010).

[24] A. S. Mayorov, R. V. Gorbachev, S. V. Morozov, L. Britnell, R. Jalil, L. A. Ponomarenko, P. Blake, K. S. Novoselov, K. Watanabe, T. Taniguchi, and A. K. Geim, Nano Lett. **11**, 2396 (2011).

[25] K. Nomura and A. H. MacDonald, Phys. Rev. Lett. **96**, 256602 (2006).

[26] J. Alicea and M. P. A. Fisher, Phys. Rev. B **74**, 075422 (2006).

[27] I. F. Herbut, Phys. Rev. B **75**, 165411 (2007).

[28] W. Bao, Z. Zhao, H. Zhang, G. Liu, P. Kratz, L. Jing, J. Velasco, D. Smirnov, and C. N. Lau, Phys. Rev. Lett. **105**, 246601 (2010).

[29] K. S. Novoselov, A. K. Geim, S. V. Morozov, D. Jiang, M. I. Katsnelson, I. V. Grigorieva, S. V. Dubonos, and A. A. Firsov, Nature (London) **438**, 197 (2005).

[30] Y. Zhang, Y.-W. Tan, H. L. Stormer, and P. Kim, Nature (London) **438**, 201 (2005).

[31] Y. Barlas, K. Yang, and A. H. MacDonald, Nanotechnology **23**, 052001 (2012).

[32] F. Zhang, D. Tilahun, and A. H. MacDonald, Phys. Rev. B **85**, 165139 (2012).

[33] See Supplemental Material at http://link.aps.org/supplemental/10.1103/PhysRevLett.117.066601, which includes Refs. [34–35], for a detailed description of the Landau levels in ABA TLG at zero electric displacement field.

[34] M. S. Dresselhaus and G. Dresselhaus, Adv. Phys. **30**, 139 (1981).

[35] L. M. Zhang, Z. Q. Li, D. N. Basov, M. M. Fogler, Z. Hao, and M. C. Martin, Phys. Rev. B **78**, 235408 (2008).

[36] Z. Papic, D. A. Abanin, Y. Barlas, and R. N. Bhatt, Phys. Rev. B **84**, 241306 (2011).